THE ASTROPHYSICAL JOURNAL, 435:668–681, 1994 November 10

MULTIPLE HIGH-VELOCITY EMISSION-LINE SYSTEMS IN THE E + S PAIR CPG 29[1]

P. MARZIANI AND W. C. KEEL
Department of Physics and Astronomy, University of Alabama, Tuscaloosa, AL 35487-0324
D. DULTZIN-HACYAN
Instituto de Astronomia, UNAM, Apartado Postal 70-264, México D. F., México
AND
J. W. SULENTIC
Department of Physics and Astronomy, University of Alabama, Tuscaloosa, AL 35487-0324
Received 1994 February 11; accepted 1994 May 9

ABSTRACT

A detailed study of the mixed-morphology galaxy pair CPG 29 (Arp 119, VV 347) shows spectacular spectroscopic peculiarities in the southern (spiral) component (Mrk 984) including a spatially resolved region, roughly aligned along the minor axis of the galaxy, with multiple emission-line components redshifted by as much as 1300 km s^{-1} with respect to the LINER nucleus. Strong [O I] λ6300 and [S II] $\lambda\lambda$6716, 6731 emission suggest shock ionization. The rest of the galaxy's disk is spectroscopically undistinguished, with emission lines characteristic of disk H II regions and, in large part, ordered rotation.

We discuss the following four possible explanations for the morphological and spectroscopic peculiarities in the spiral: (1) a superwind scenario, supported by the high FIR luminosity of the spiral and by emission-line activity similar to that observed in FIR-strong galaxies; (2) motion of the spiral through a hot, relatively dense intergalactic medium, possibly associated with the elliptical, that could affect the star formation and create a brightened disk rim; (3) a faint companion in direct collision with the disk, at $\Delta v_r \sim 1000$ km s^{-1}, that would straightforwardly explain the existence of the different redshift systems; and (4) a pole-on collision by the elliptical, that could produce the disturbed morphology and other properties of the spiral.

The elliptical/spiral pole-on collision explains the high-velocity line-emitting regions as tidally stripped gas and accounts for the presence of gas ionized by moderate velocity shocks. The morphology of Mrk 984 is consistent with a ring galaxy and numerical simulations suggest that the elliptical can emerge unscathed from a relatively high velocity crossing.

Subject headings: galaxies: individual (Markarian 984, CPG 29) — galaxies: interactions — galaxies: kinematics and dynamics

1. INTRODUCTION

Gravitational interaction between galaxies is responsible for a wide variety of phenomena. Many morphological peculiarities in spiral galaxies, such as bars, tails, and external rings, have been related to tidal effects (Toomre & Toomre 1972; Lynds & Toomre 1976; Elmegreen, Elmegreen, & Bellin 1991). Comparisons of interacting and isolated galaxy samples suggest that spectroscopic and photometric properties are also modified in interacting systems. Galaxies in the Arp (1966) atlas have excess radio continuum emission (Sulentic 1976) and a wider dispersion in *UBV* colors than isolated galaxies (Larson & Tinsley 1978). Hα luminosities in disks and nuclei of interacting systems are on average much higher ($\times 10$) than in isolated galaxies (Kennicutt et al. 1987; Bushouse 1987). Far-IR emission is also strongly enhanced in interacting galaxies (Bushouse 1987; Xu & Sulentic 1991). All these results can be linked to an enhanced star formation rate (SFR) in interacting galaxies.

Gravitational interaction may also be the ultimate triggering mechanism of nonthermal nuclear activity. Dahari (1985) and Rafanelli & Marziani (1992) found a significant excess of interacting systems among Seyfert galaxies. It is still unclear how interaction may ultimately lead to the production of an active nucleus. An evolutionary link between a starburst and the origin of an active nucleus is fashionable (either remnants of evolved massive stars may coalesce to form a massive black hole [e.g., Weedman 1983] or mass loss may provide accreting matter, if the black hole was formed earlier [Norman & Scoville 1988; Heckman, Armus, & Miley 1990]).

Object 29 in the Catalog of Isolated Pairs of Galaxies (CPG 29; Karachentsev 1972), also known as VV 347 and Arp 119, is a spiral + elliptical pair (components hereafter referred to as CPG 29S and CPG 29N or S and E for brevity) of galaxies, with projected component separation of approximately 1′. The southern component (0116+121 ≡ CPG 29S ≡ Mrk 984 ≡ UGC 849) has been classified as type Sdm pec in RC3 (de Vaucouleurs et al. 1991). The peculiarities in S are not confined to morphology but include an unusual emission-line spectrum. The broad and complex line profiles of this object were first noted by Osterbrock & Dahari (1983). S has been cataloged as a Seyfert 2 galaxy (Artyuk et al. 1982), but the nuclear ionization level is too low for it to be considered as a *classical* Seyfert 2 (Osterbrock & Dahari 1983). The line ratios are, at first glance, more typical of a LINER (Dahari & De Robertis 1988; Mazzarella & Boroson 1993).

The most puzzling aspect presented in this paper results from long-slit spectroscopy where we find (at least) four red-

[1] Based in part on data collected at the European Southern Observatory, La Silla, Chile; Kitt Peak National Observatory, National Optical Astronomy Observatories, operated by AURA under cooperative agreement with the NSF; Lowell Observatory, Flagstaff, Arizona; Observatorio Astronomico Nacional, San Pedro Martir, Baja California, Mexico; and Special Astrophysical Observatory, formerly USSR Academy of Sciences.

shift systems covering a range $\Delta v_r \approx 1300$ km s^{-1} in excess of the radial velocity of the underlying galaxy. Emission in the high-velocity systems occurs in a region roughly aligned close to the minor axis of the galaxy, associated with the nucleus of Mrk 984, and a northern blob (see Fig. 1).

In § 2 we describe new imaging and spectroscopic observations, reduction, and data analysis. Morphology, velocity curves, and properties of the line-emitting regions are presented in § 3. In § 4 we analyze the ionization mechanism, estimate the galactic masses, and suggest a hint to the star formation history for S. In § 5 we discuss four possible explanations for this remarkable system.

2. OBSERVATIONS AND DATA REDUCTION

2.1. *Imaging*

The first part of Table 1 summarizes the imaging observations. The KPNO *B* and *V* images were obtained as part of a survey of mixed pairs by N. Sharp and J. W. Sulentic. Images in the red were obtained at Lowell Observatory. A filter of FWHM 75 Å centered near 6900 Å traced Hα and [N II] line emission. An emission-line image was produced by subtraction of a scaled *R* image, instead of pure continuum, giving the right emission-line morphology but underestimating the flux by a known factor, given the ratio of the two bandwidths.

2.2. *Long-Slit Spectroscopy*

A journal of spectroscopic observations is given in the second part of Table 1. The 2.1 m (f/7.5) telescope of the Mexican Observatorio Astronomico Nacional located on Sierra San Pedro Martir (Baja California, Mexico) was equipped with a Boller & Chivens spectrograph and a 600 lines mm^{-1} grating (2″.5 slit). The KPNO 2.1 m telescope was used with the Gold Camera spectrograph (2″.5 slit). The ESO 1.5 m

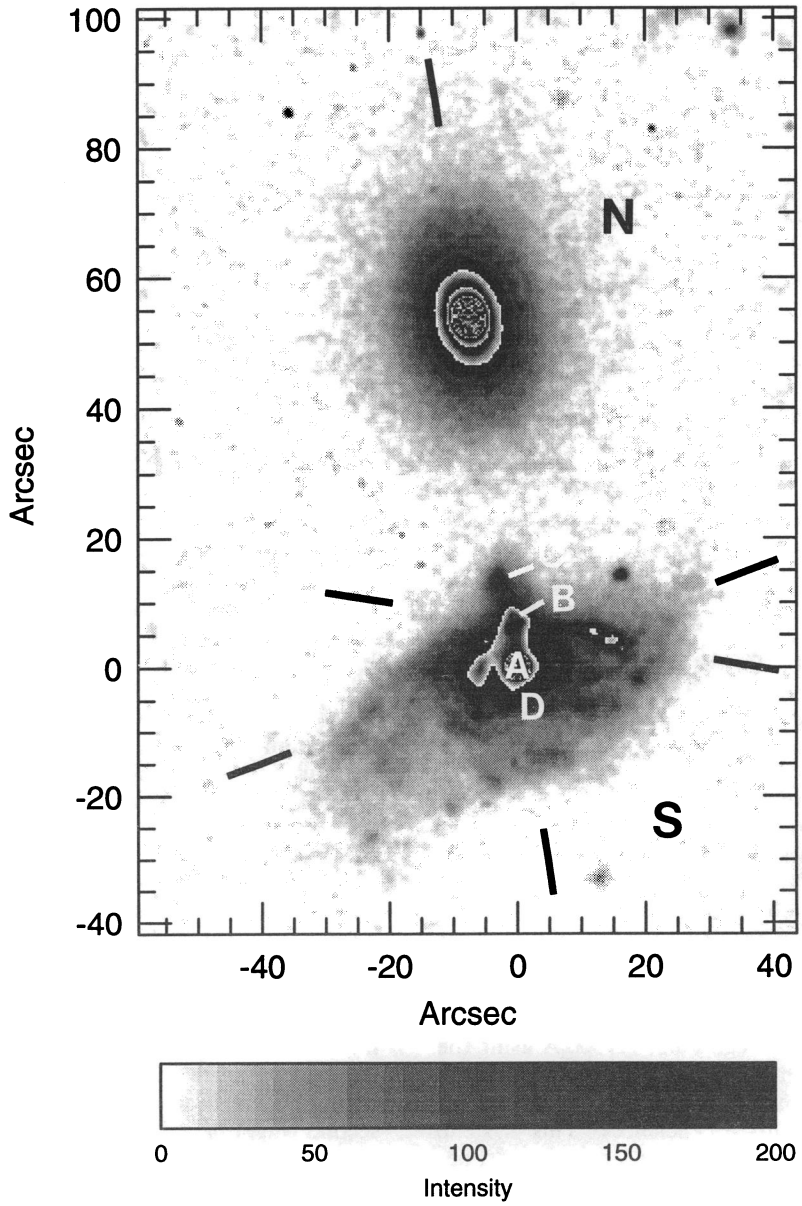

FIG. 1.—*V*-band image of CPG 29. North is at the top, and east is to the left. The ticks identify the three slit configurations used to obtain the spectra. Location of regions A, B, C, D are also marked.

TABLE 1

JOURNAL OF OBSERVATIONS

Observatory	Telescope	Detector	Date	U.T.	Exposure Time (minutes)	Filter	Scale (arcsec pixel^{-1})	Dispersion (Å mm^{-1})	P.A.	Spectral Range (Å)
KPNO	2.1 m	Tek 512 × 512	1986 Nov 29	05 59	20	*B*	0.3429	...	...	...
	2.1 m	Tek 512 × 512	1986 Nov 29	04 16	15	*V*	0.3429	...	...	...
Lowell	1.1 m	TI 800 × 800	1991 Sep 12	08 07	90	Hα	0.708	...	...	...
	1.1 m	TI 800 × 800	1991 Sep 12	09 40	30	*R*	0.708	...	...	...
KPNO	2.1 m	TI 800 × 800	1990 Nov 23	02 17	45	...	0.782	85	8°	6140–7160
SPM	2.1 m	Thompson 385 × 576	1991 Dec 6	05 51	40	...	0.873	114	7	6320–7450
	2.1 m	Thompson 385 × 576	1991 Dec 6	06 58	30	...	0.873	114	116	6320–7450
ESO	1.5 m	FA2K	1992 Jul 1	09 44	60[a]	...	0.68	159	3[b]	3670–7580
	1.5 m	FA2K	1992 Jul 2	09 07	80[a]	...	0.68	159	81[c]	4530–7580
KPNO	2.1 m	Ford 1024 × 3072	1992 Nov 14	05 46	60	...	0.782	85	82	4470–8330

[a] Sum of two consecutive exposures.
[b] Focusing problem; extracted only regions A and B.
[c] Focusing problem; used only for confirmatory purposes.

telescope was equipped with a Boller & Chivens spectrograph and 400 lines mm^{-1} grating.

All slit spectra were reduced in essentially the same way. Frames were bias subtracted and flat-field corrected. Wavelength calibration, from helium-argon spectra obtained after each exposure, gave an rms precision ≤ 0.05 Å. Spectral resolution (FWHM) was 3.8 Å (KPNO), ≈ 5 Å (SPM), and ≈ 4 Å (ESO). The spectra were rebinned to linear wavelength scales and corrected for cross-dispersion distortion, and finally extinction corrected and flux calibrated. Standard stars were not observed on the same nights as the CPG 29 data at ESO and KPNO, so the response curve was computed from stars observed on different nights of the same runs. We can be confident that large errors in the spectrophotometry are absent, since the continuum fluxes of the 1990 and 1992 KPNO spectra, and of the ESO spectra for A and B, agree well. The accuracy in the absolute continuum fluxes at 6500 Å is estimated to be $\sim 20\%$. Continuum fluxes for A (P.A. = 7°) obtained at SPM are about 25% lower than those obtained from the KPNO and ESO spectra. We did not scale the SPM fluxes (reported in Tables 2 and 3) to the average continuum value. The reader must be aware that an underestimate of the flux as large as 25% is possible for the emitting regions on the SPM spectra reported in Tables 2 and 3 (P.A. = 116°).

Some emission-line fluxes disagree markedly (see Table 2), most probably due to the peculiar extended emission in this object. The flux of the Hα + [N II] λλ6548, 6583 blend in the circumnuclear region is comparable to that of the nucleus. A slight misplacement or a change of orientation or atmospheric seeing might change the emission-line fluxes appreciably. This is especially true for fluxes of the extranuclear regions closest to A. The uncertainty of the line fluxes measured in these regions is probably larger than that associated with the other nuclear emitting regions, and is estimated to be around 40%.

2.3. *Area Spectroscopy*

Part of S was observed in the region 6200–7000 Å using the multipupil fiber spectrograph (MPFS) at the 6 m telescope (BTA) of the Special Astrophysical Observatory (SAO) of what was then the USSR Academy of Sciences. This system, described by Afanasiev et al. (1990), uses a lens-coupled fiber array to simultaneously measure the spectra of an 8 × 12 array of 1.25 arcsec^2 apertures. The detector was a 512 × 512 TV-based photon-counting system. Monochromatic maps of the continuum and line features were produced.

3. RESULTS

3.1. *Morphology*

The nuclei of S and E are separated by $54'' \pm 0''.2$, or a projected linear separation of 38 h^{-1} kpc (for $H_0 = 100 \times h$ km s^{-1} Mpc^{-1} so that $1'' \approx 688\ h^{-1}$ pc; see Fig. 1. Markarian 983 is located approximately 2'.5 south of S. It shows a heliocentric $v_r \approx 14{,}400$ km s^{-1}; Palumbo, Tanzella-Nitti, & Vettolani 1983), consistent with a common distance for this galaxy and CPG 29. Mrk 983 has been described as having multiple nuclei or hot spots (Mazzarella, Bothun, & Boroson 1991; Mazzarella & Boroson 1993). It is within the field of our Lowell images and in *R* shows what may be face-on spiral structure with a pronounced bright knot along an armlike feature west of the nucleus. This knot is by far the dominant source of Hα emission in Mrk 983, with weaker emission at the nucleus and along the apparent western arm.

The spiral component subtends $\approx 72'' \times 32''$ ($\approx 49 \times 22\ h^{-1}$ kpc). The southeastern part of S shows fairly regular spiral structure, typical for Sc galaxies. Our new images suggest an Sc peculiar type for S. The axial ratio is consistent with an inclination $i \sim 63°$ (the UGC values imply $i = 66°$). Direct estimation of the inclination from the axial ratio may be misleading because of either warping of the disk or a tilted outer ring (see § 5.3.). A most relevant *morphological* peculiarity in S is the presence of two knots to the north of A and toward the nucleus of E—knot B ($m_B \approx 20.0$, $d_{BA} \approx 6''$) and knot C ($m_B \approx 21.0$; Mazzarella & Boroson 1993, $d_{AC} \approx 13''.6$; Fig. 1). B and C are located approximately along the separation vector of the pair. B appears starlike on the blue frame (see Fig. 2) and becomes distinctly elongated on the *V* image (Fig. 1). At least two, and more likely three, ringlike structures might be present in S. An inner ring surrounds the nucleus A at $r = 6''$–$7''$. Knot B is superposed on this feature, but the ring itself is not a site of strong Hα emission (see Fig. 2). The bright arc R is a part of a second ring at $d \approx 14''$ from the nucleus. A line of faint knots, probably H II regions, that skirts the southern edge of the disk, and the arc on the northeast visible on Fig. 1, could be a third ringlike feature (§ 5.3).

TABLE 2

S ≡ MARKARIAN 984: EMISSION-LINE FLUXES AND WIDTHS OF REGIONS WITH MULTIPLE LINE[a] PROFILES

		TOTAL		[1]			[4]		
REGION	IDENTIFICATION	Flux	EW	Flux	EW	FWHM	Flux	EW	FWHM
A[b]	[S II] λλ6716, 6731	25	39	8.4	14	380	...	...	380
	[N II] λ6583	22.4	32	10.3	15	370	4.02	6	370
	Hα	27.0	40	9.6	14	400	5.73	8.5	400
	[N II] λ6548	7.6	11	3.4	5	370	1.34	2	370
	[O I] λ6363	<2.8	<4	...	...	...	...	...	...
	[O I] λ6300	6.2	10	3.4	2.5	410	1.87	2.2	410
A[c]	[S II] λλ6716, 6731	14.5	62	...	...	...	...	...	...
	[N II] λ6583	14.4	62	8.46	36	≲220	<2.27	9.7	≲220
	Hα	8.57	32	2.93	12.5	≲220	3.36	14.5	≲220
	[N II] λ6548	4.89	21	2.87	12.2	≲220	0.76	3.3	≲220
	[O I] λ6300	4.68	20	0.48	4	280	1.59	6.5	280
B[b]	[S II] λλ6716, 6731	18.4	52	...	...	...	...	...	...
	[N II] λ6583	14.7	45	2.45	...	>180	5.1	16	340
	Hα	29.6	94	5.31	17	240	12.8	40	240
	[N II] λ6548	5.0	15	0.83	...	180	1.73	5	340
	[O I] λ6300	4.4	12	0.42	1	240	1.52	4	240
B[d]	[S II] λλ 6716, 6731	21.0	57	8.34	22	270	...	...	270
	[N II] λ6583	18.5	39	6.50	18	250	5.34	14	340
	Hα	32.0	81	11.8	30	210	10.7	27	250
	[N II] λ6548	6.2	13	2.5	6	250	1.81	5	340
	[O I] λ6363	<2	<5	...	...	...	...	...	...
	[O I] 6300	4.95	14	...	...	...	...	...	...
	[O III] λ5007	12.36	35	4.20	12	375	4.85	14	385
	Hβ	11.93	33	4.35	12	330	4.97	14	385
D[b]	[S II] λλ6716, 6731	22.2	47	...	...	...	...	...	...
	[N II] λ6583	21.0	45	13.8	30	375	2.15	5	310
	Hα	17.8	40	9.76	22	425	4.29	10	430
	[N II] λ6548	7.2	16	4.7	10	375	0.75	1.8	360
	[O I] λ6363	...	...	...	...	...	...	...	...
	[O I] λ6300	5.0	12	2.5	6	360	0.94	2.5	360
F[c]	[S II] λλ6716, 6731	4.53	41	...	...	...	...	...	...
	[S II] λ6731	...	...	...	...	...	...	...	...
	[S II] λ6716	...	...	...	...	...	...	...	...
	[N II] λ6583	5.89	53	...	...	...	...	...	...
	Hα	5.25	48	...	...	...	...	...	...
	[N II] λ6548	2.00	18	...	...	...	...	...	...
	[O I] λ7300	1.91	17	...	...	...	...	...	...

[a] Fluxes are in units of 10^{-15} ergs cm^{-2} s^{-1}; EW are in units of Å and FWHM are in units of km s^{-1}.
[b] At P.A. = 8°.
[c] At P.A. = 116°.
[d] At P.A. = 81°.

Figure 2 compares the inner regions of S on the Hα and B images. Two intriguing results emerge: (1) the nucleus (A) on the blue image lies between two knots of Hα emission, but close to the (fainter) southern one. A further look at the blue image shows that A is partially resolved and slightly fainter on the north east side. (2) The blue image shows a knot toward the east of the nucleus that has no obvious counterpart on the Hα image. Conversely, the Hα images shows emission to the south without obvious counterpart in the blue.

Geometric and luminosity profiles for E are shown in Figure 3 for both the *B* and *V* images. There is no evidence for variation in the isophotal ellipticity (Fig. 3, *middle panel*) outside of the 2″ seeing disk. The major axis orientation (Fig. 3, *upper panel*) shows a small rotation from ≈14° down to ≈8° at $d \approx 15''$, with a global change of $|\Delta \text{ P.A.}| \lesssim 10°$. The surface brightness profile (given in arbitrary units in the bottom panel of Fig. 3) shows minor deviations from an $r^{-1/4}$ profile including a small ripple at $d \approx 16''$, followed by a steepening outward. The isophotal centroid is constant with intensity to within ≈1.″5.

3.2. *Definition of the Line-emitting Regions*

Line-emitting regions were isolated to match the most prominent morphological features observed in the *B* and *V* images. The definitions are based on a careful analysis of the cross-dispersion profile of the Hα + [N II] λλ6548, 6583 blend, and the continuum at ≈6500 Å. The definition of each emitting region can be found on Figures 4, 5, and 6. The heliocentric v_r for each region was estimated from several lines among [N II] λ6583, Hα, Hβ, [O III] λ5007, [O I] λ6300. Blending prevented us from measuring some of the lines in particular regions. Heliocentric radial velocities estimated from different lines are the same within the observational uncertainties for all components over all the regions we identified. In particular, the v_r estimated from [O III] λλ4959, 5007 is in agreement with v_r estimated from the Balmer lines. Table 3 reports fluxes and widths of regions having single-peaked emission-line profiles.

3.3. *Extended Emission*

The most striking feature in the spectra taken at P.A. = 8° are the apparently broad (FWHM) ~ 1200 km s^{-1}), multi-

TABLE 3

S ≡ MARKARIAN 984: EMISSION-LINE FLUXES AND WIDTHS OF REGIONS WITH SINGLE-PEAKED EMISSION-LINE PROFILES[a]

	I[b]			R[c]			R ≡ B. ARC[b]			C[d]		
IDENTIFICATION	Flux	EW	FWHM	Flux	EW	FWHM	Flux	EW	FWHM	Flux	EW	FWHM
[S II] λ6731	1.81	11	≲170	2.01	15	240	2.24	13	≲170	1.53	21	270
[S II] λ6716	2.20	14	≲170	1.59	12	230	3.00	17	≲170	2.06	27	270
[N II] λ6583	4.02	24	≲180	3.21	26	≲220	4.58	28	≲180	1.81	23	≲220
Hα	9.25	61	≲180	6.06	49	≲220	13.1	81	≲180	6.35	65	≲220
[N II] λ6548	1.67	12	≲180	1.10	9	≲220	1.82	11	≲180	...	...	...
[O I] λ6300	<0.7	<5	...	0.46	3	...	0.4	2	≲180	1.27	16	420:
[O III] λ5007	1.12	8	280	...	...	...	1.30	5.5	215	...	...	...
Hβ	1.75	9	205	...	...	...	4.64	23	265	...	...	...

	J[b]			K[b]			M[c]			T[c]		
IDENTIFICATION	Flux	EW	FWHM	Flux	EW	FWHM	Flux	EW	FWHM	Flux	EW	FWHM
[S II] λ6731	1.23	12	≲170	0.63	7	175	...	...	...	0.23	4.5	≲220
[S II] λ6716	1.61	16	≲170	0.98	11	175	...	...	...	0.25	4.1	≲220
[N II] λ6583	2.82	30	≲180	1.33	16	170	<1.91	7	265	0.71	17	320:
Hα	7.24	73	≲180	3.97	48	170	2.95	12	≲220	2.03	49	≲220
[N II] λ6548	0.96	9	≲180	...	...	...	...	...	...	...	...	...
[O I] λ6300	0.3	3	≲180	...	...	...	...	...	...	...	...	...
[O III] λ5007	0.66	5	≲220	0.95	7.5	190	...	...	...	...	...	...
Hβ	1.80	13	210	1.13	9	≲220	...	...	...	...	...	...

[a] Fluxes are in units of 10^{-15} ergs cm^{-2} s^{-1}; EW are in units of Å, and FWHM are in units of km s^{-1}.
[b] P.A. = 81°.
[c] P.A. = 116°.
[d] P.A. = 8°.

peaked emission-line profiles. Broad profiles are observed for [O I] λλ6300, 6363; [O III] λ5007; Hβ, Hα, [N II] λλ6548, 6583 and [S II] λλ6716, 6731. They are seen in A and extend north-south for approximately 10″ (regions A, B, and D). This extended region appears in the spectra at P.A. = 3° and 8°; see Fig. 4). At P.A. = 116°, broad line profiles are observed only from A and in the region immediately east of the nucleus (region F; Fig. 5). The spectra taken at P.A. = 81° (Fig. 6) show multipeaked profiles only at knot B.

The profile variation of the blend Hα + [N II] λλ6548. 6583 along the slit at P.A. = 8° is shown in Fig. 7. Analysis of the Hα + [N I] λλ6548, 6583 profile in A and in the surrounding emission region shows that each line of the blend is made up of four velocity components. We have numbered the line components from [1] to [4] in order of increasing radial velocity. Evidence in favor of multipeaked lines comes from the appearance of [N II] λ6583 components [2], [3], and [4] line in the region of B and, in part, A (Fig. 7). It is likely that the subdivi-

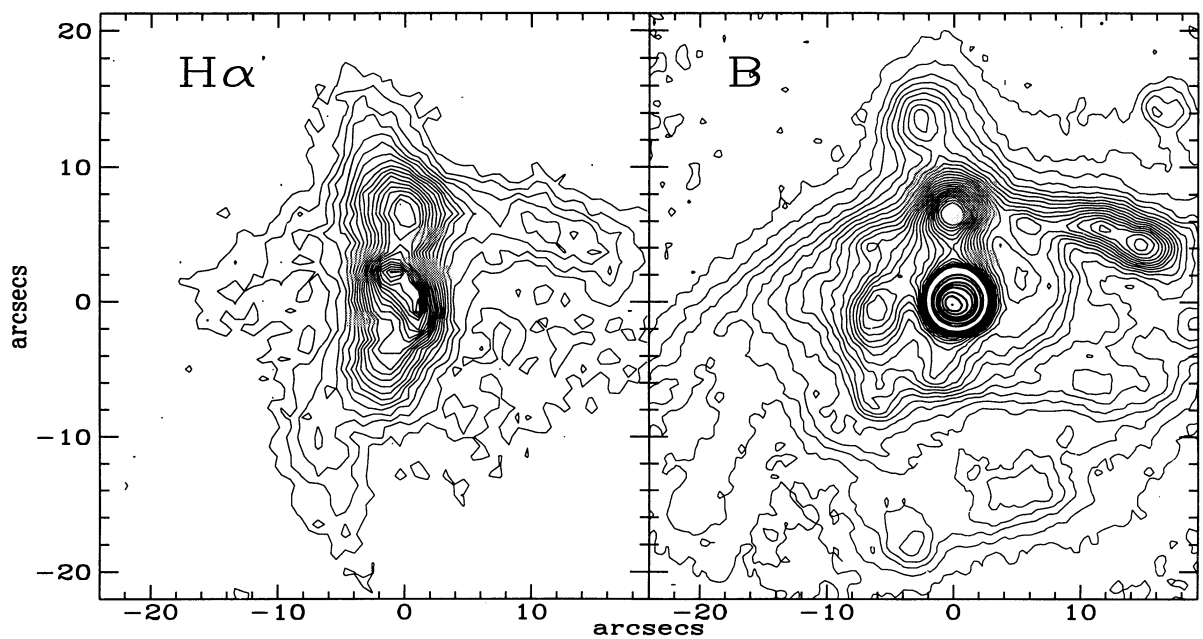

FIG. 2.—Contour plots of the inner regions of Mrk ≡ 984 S, from the B (*right*) and Hα (*left*) images. North is at the top, and east is to the left.

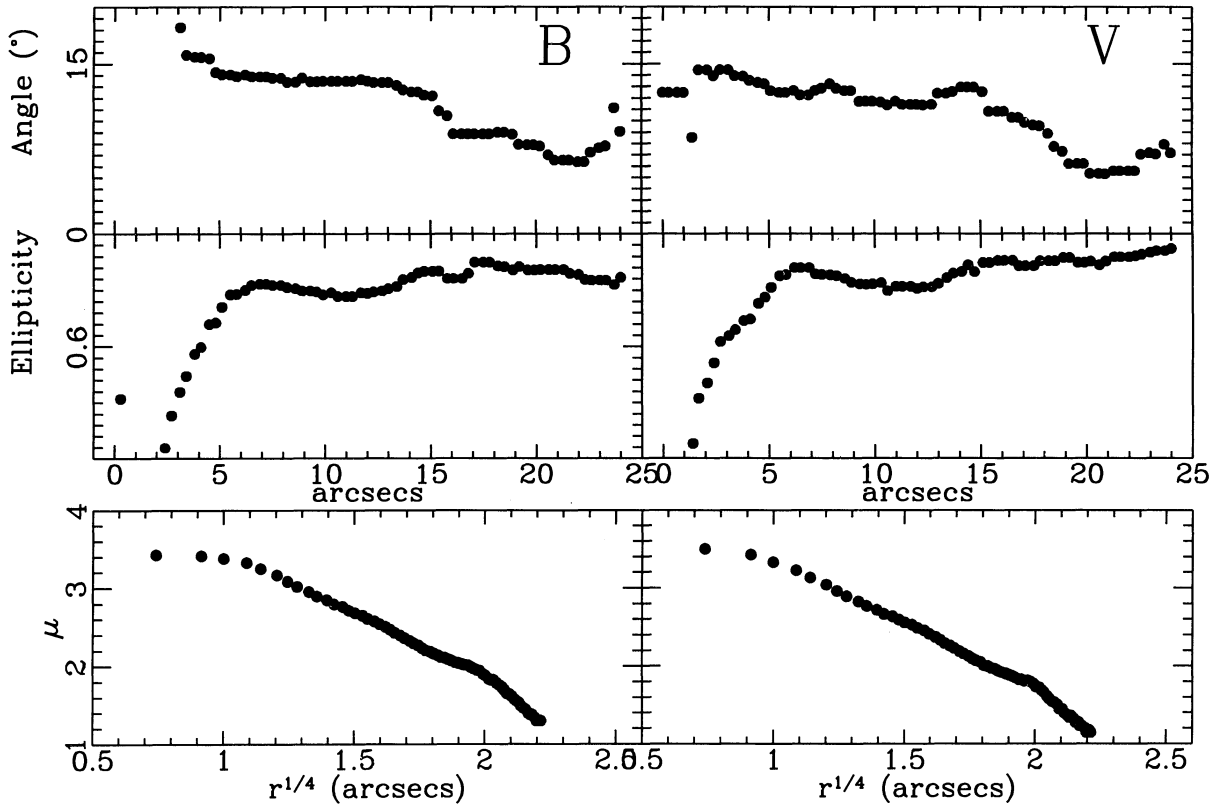

FIG. 3.—Geometrical properties of the elliptical galaxy, CPG 29N, *left*: *V* image; *right*: *B* image. *Top panel*: P.A. of the major isophotal axis as a function of radius (in arcseconds); *middle panel*: ellipticity; *bottom panel*: surface brightness (in arbitrary units) vs. $r^{1/4}$.

sion into four redshift systems is an oversimplification. Scans corresponding to A and D (Fig. 7) suggest that another component displaced by $v_r \sim 80$ km s^{-1} from [1] may also be present.

3.3.1. *Analysis of the* Hα + [N II] λλ6548, 6583 *blend*

Although the blending is severe, multicomponent fitting with a single FWHM value proved to be reliable (i.e., results did not depend upon details in the placements of the continuum or initial estimate of the peak positions). We detail our procedure in the following paragraph.

Component [1] ($V_r \approx 14250$ km s^{-1}) of [N II] λ6548 is not contaminated by any other line, so we constructed a template [N II] λ6583 [1] using a Gaussian profile of the same width, taking advantage of the fact that the intensity ratio [N II] λ6548/[N II] λ6583 is fixed. Components [2], [3], and [4] of [N II] λ6583, although heavily blended, are not contaminated by other lines. A deblending procedure was applied to these three lines as a first step. After deblending of [N II] λ6583, templates were constructed for [N II] λ6548 at the expected wavelengths. [N II] emission was subtracted from the original spectrum, leaving a *pure* Hα blend. A multi-Gaussian deconvolution procedure was then applied to the Hα blend as well. The strength and width of the [1] and [4] components were found to be well constrained; the uncertainty due to the deblending procedure is estimated to be ≈10% and should be added to the uncertainty in the flux calibration. We report the decomposition results in Table 2 where we give flux, EW, and FWHM (only for [1] and [4]; on results are given for F, since the S/N ratio is low) and the total flux and EW in each line (the total flux of the four components) for all regions where emission lines show composite profiles.

3.4. *Emitting Regions at P.A.* = 8°

A.—The overall spectrum of A is shown in Figure 8. It is more suggestive of FIR-loud galaxies or LINERs than of classical starburst and Seyfert galaxies. The width of the [O I] λ6300 line is for instance similar to the width in NGC 1068, the prototypical Seyfert 2 galaxy, but the ratio [O III] λ5007/Hβ ∼ 1 is too low for a Seyfert classification (Osterbrock 1978). The Hα + [N II] λλ6548, 6583 blend appears smoother than in B and blending of the various components is more severe in this region allowing almost no discrimination of the suspected multiple components. The FWHM ∼ 400 km s^{-1} of each component is somewhat larger here than in the other regions.

The radial velocity of the underlying galaxy estimated from the Na D line is $v_r \approx 14{,}200$ km s^{-1}. The velocity curve at 0″ (P.A. = 116°) gives a consistent value, $v_r \approx 14{,}200$ km s^{-1}. These values are also consistent with the H I profile reported by Bothun et al. (1984), from which we estimated a systemic radial velocity ≈14,198 km s^{-1}. The RC3 reports v_r(H I) ≈ 14,265 km s^{-1}, but the H I profile of S is disrupted on the long-wavelength side, making a mean velocity, uncertain. The multiple line components show $v_r \approx 14{,}250$ [1], 14,700 [2], 15,000 [3], and 15,450 [4] km s^{-1}. The lowest velocity in the multiple emission region is similar to the v_r of the underlying galaxy. The continuum is rising toward the blue in F_λ, suggesting an enhanced star formation rate (§ 4.3).

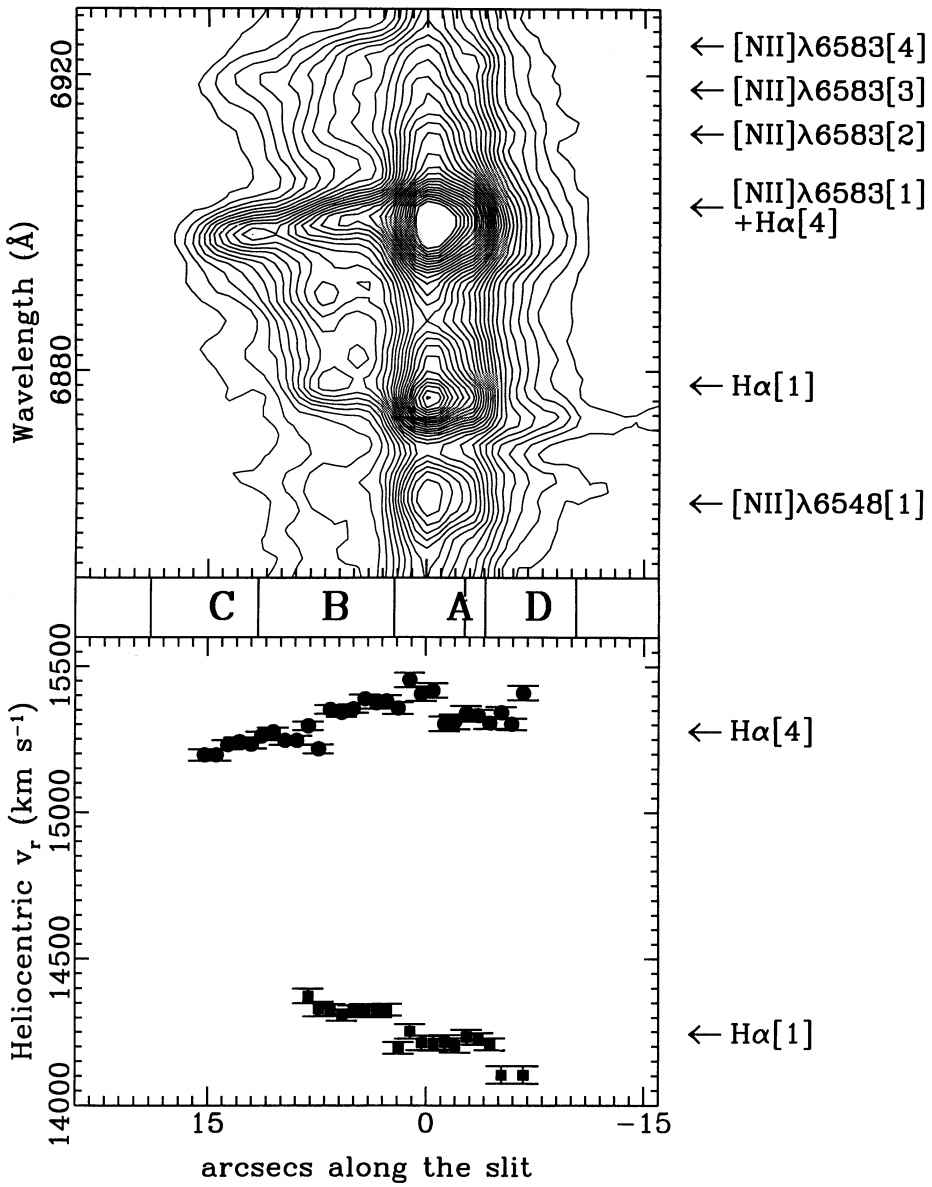

FIG. 4.—Isophotal contours of the Hα + [N II] λλ6548, 6583 emission lines of S at P.A. = 7°. Horizontal scale is arcseconds along the slit; vertical scale is wavelength in Å. The origin of the horizontal scale has been set at the centroid of the continuum at ≈6450 Å (rest frame). Note the off-centering of the emission-line blend with respect to the continuum. Radial velocity curves. *Filled circles*: redshift system [1] (see text); *filled squares*: redshift system [4]. Vertical scale is heliocentric radial velocity in km s^{-1}.

B.—The emission-line luminosity of B is comparable to that observed in A, but the underlying continuum is significantly weaker. We detected no absorption lines. The emission line ratios also differ from those of A. Both components [1] and [4] show [N II]/Hα consistent with stellar photoionization, but the strength of [O I] λ6300, especially in [4], may require some additional source such as shocks. Radial velocities of the four components are $v_r \approx$ 14,350 [1], 14,690 [2], 14,960 [3], and 15,370 [4] km s^{-1}.

C.—Emission-line profiles are single peaked and barely resolved in our spectra. Emission-line ratios are typical of H II regions.

D.—This is a site of strong off-nuclear line emission. The ratio [N II] λ6583/Hα ~ 1.5 for [1] is larger than in A. The redshifted line components are weaker compared to [1] (e.g., Hα luminosity of [4] is only ~0.5 that of [1]) than seen at A. The maximum value of the ratio [N II] λ6583/Hα in component [1] is seen at D. On D the redshifted emission fades rapidly, giving the appearance of a broad wing to the lines (see Fig. 7). Line components v_r are 14,320 [1], 14,870 [2], 15,130 [3], and 15,380 [4] km s^{-1}.

CPG 29N ≡ *E*.—We derive $v_{r,E} = 15{,}000 \pm 30$ km s^{-1} from the Na D line for the recessional velocity of E, in agreement with Tifft (1982). Karachentsev, Sargent, & Zimmermann (1979) give $v_{r,E} \approx$ 14,806 km s^{-1}, while Karachentsev (1980) gives 14,429 km s^{-1}. We note that the redshift given in Karachentsev (1987) $v_{r,E} \approx$ 14,569 km s^{-1} is a typographical error. Mazzarella & Boroson (1993) recently report a surprising

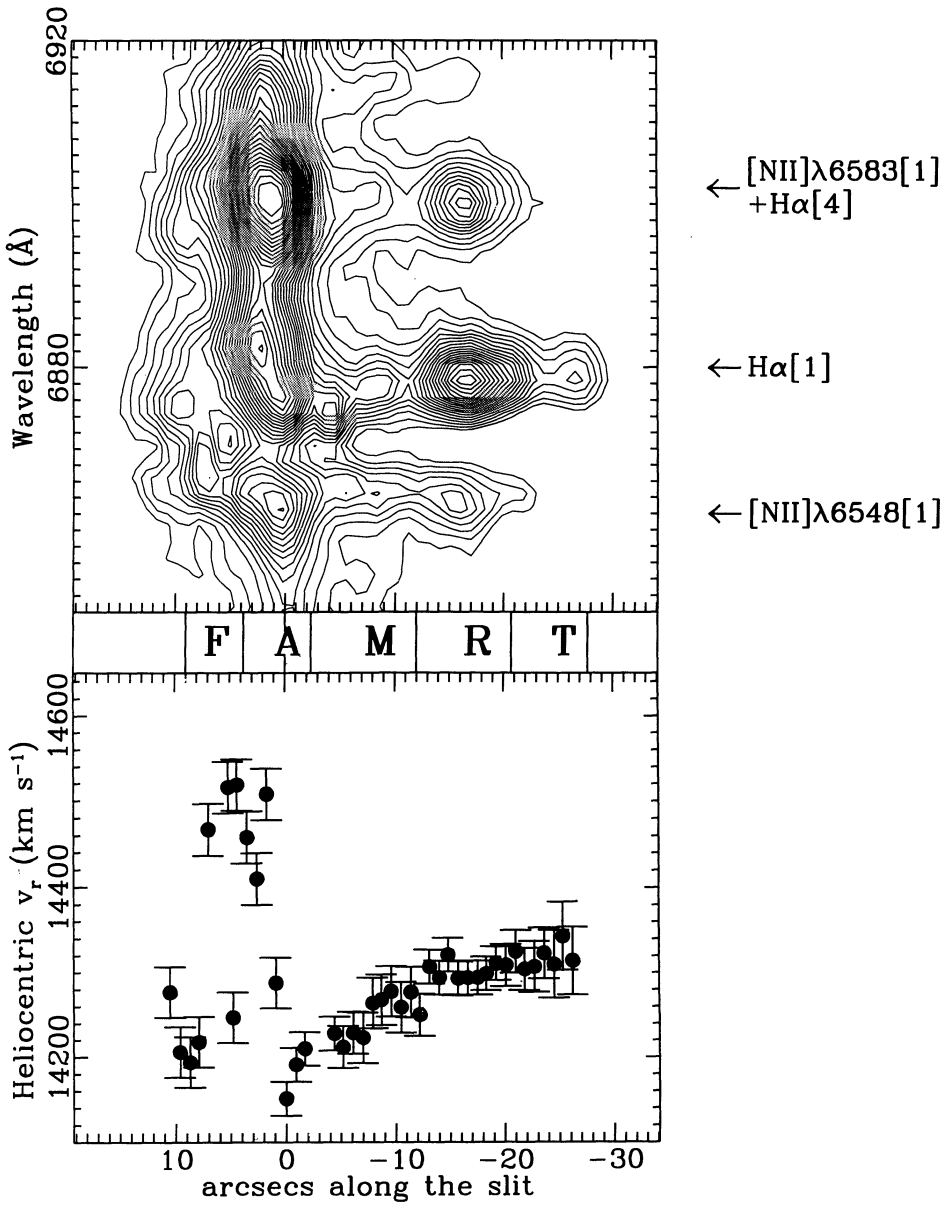

FIG. 5.—Isophotal contours of the Hα + [N II] λλ6548, 6583 extended emission of S at P.A. = 116°. Horizontal scale is arcseconds along the slit; vertical scale is wavelength in Å. The origin of the horizontal scale has been set at the centroid of the continuum at ≈6450 Å (rest frame). Note the off-centering of the emission-line blend with respect to the continuum. Radial velocity curve; Vertical scale is heliocentric radial velocity in km s^{-1}.

$v_{r,E} \approx 14{,}553$ km s^{-1}. A check of the frame that contains both E and S (P.A. = 8°) confirms a shift in the two spectra at Na D that is consistent with a velocity difference $\Delta v_{r,E-S} \gtrsim 700$ km s^{-1}.

3.5. *Velocity Curves*

Velocity curves from our long-slit spectra are given in Figures 4, 5, and 6, along with two-dimensional contour displays of the data. The spatial zero points are set from the continuum peaks of the nucleus (A) for Figures 4 and 5 and from knot B for Figure 6. We will note here some of the most important features of the velocity structure in each case.

P.A. 116°.—This is the major axis of S. The western part of the disk has a plausible rotation curve for a typical spiral, rising rapidly from the nucleus. The central velocity may be affected by the presence of systems [2] and [3]; [4] is well seen near the nucleus proper and is not plotted in the velocity slice. The contour representation shows that the peak emission in [4] is displaced by about 3″ west of the continuum peak of the nucleus A.

P.A. 8°.—The slit passed through the nuclei of both S and E. Only S is shown in Figure 4. The anomalous emission-line systems appear to best advantage in this orientation, and systems [1] and [4] can be traced in detail. Velocity gradients are resolved in both systems and at this position angle are almost along the projected minor axis of S. This may be evidence for noncircular motion in the disk gas, since simple deprojection gives implausibly large velocities within the disk plane.

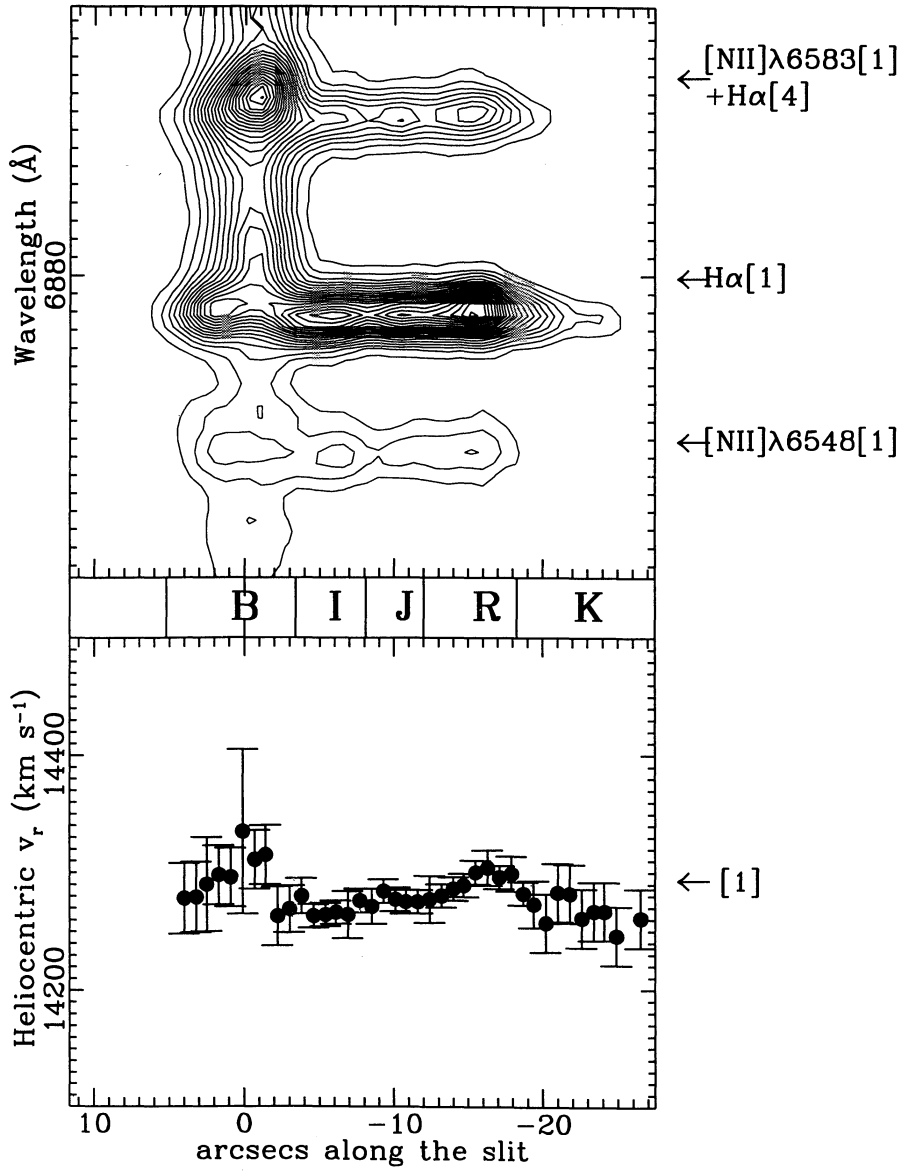

FIG. 6

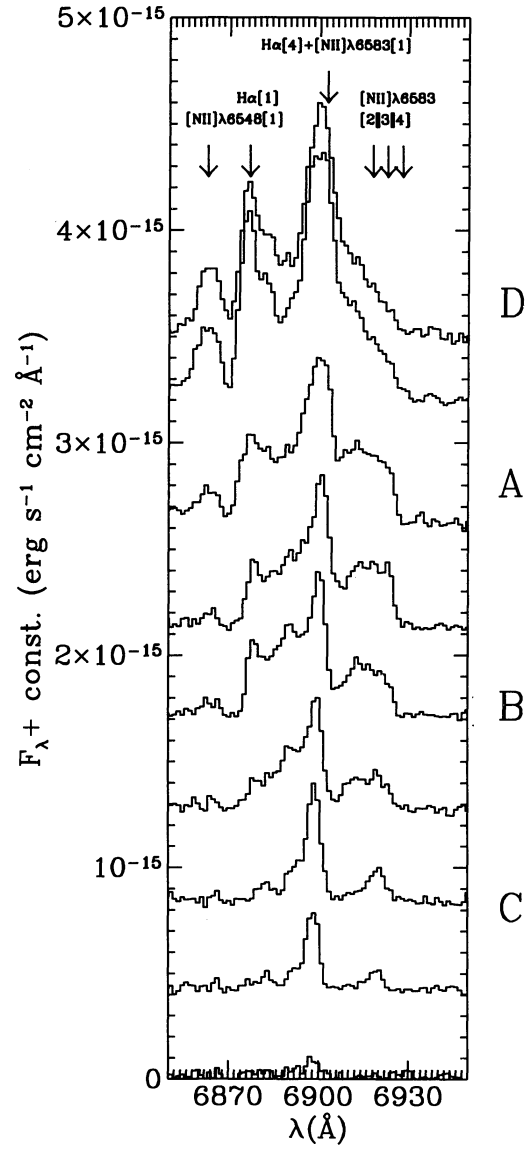

FIG. 7

FIG. 6.—Isophotal contours of the Hα + [N II] λλ6548, 6583 extended emission at P.A. = 81°, off-centered by approximately 5″.6 from the nucleus of S (e.g., with the slit centered on the brightest blob [B] and roughly aligned with the bright arc labeled as R). Horizontal scale is arcseconds along the slit; vertical scale is wavelength in Å. The origin of the horizontal scale has been set at the centroid of the continuum at ≈6450 Å (rest frame).

FIG. 7.—Extracted spectra of the Hα + [N I] λλ6548, 6583 blend along the slit at P.A. = 8°. Each spectrum corresponds to a spatial increment of approximately 2″.5. Three line components of [N II] λ6583 form the "boxy" blend to the red. The arrows indicate the wavelengths of the [N II] λ6548 [1] and of the [N II] λ6583 [2], [3], [4] components.

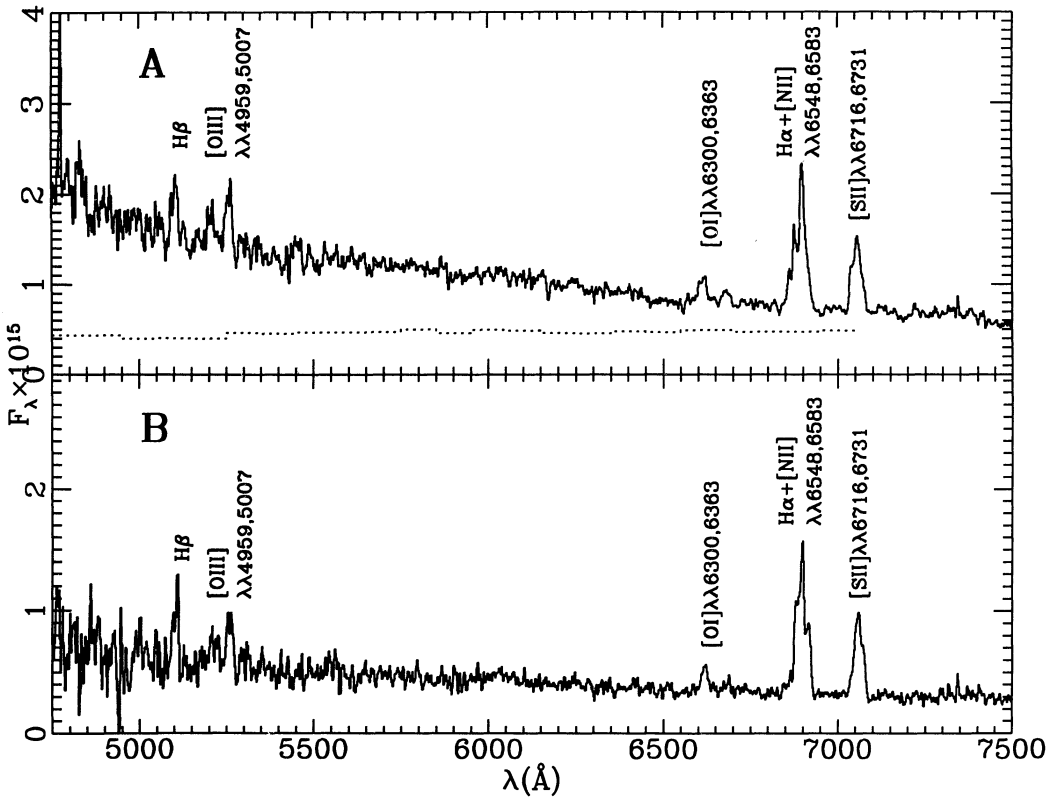

FIG. 8.—Spectra of components A and B. Horizontal scale is wavelength in Å; vertical scale is specific flux. The dotted line in the spectrum of A is the assumed continuum of the old stellar population.

P.A. 81°.—This observation includes knot B and is roughly tangent to the NW spiral arm. The anomalous systems are confined to a small region around B, with the spiral arm showing small-amplitude structure not unusual for large spirals.

4. DIRECT IMPLICATIONS

4.1. *Ionization Mechanisms*

Figure 9 presents diagnostic diagrams, according to the prescription of Veilleux & Osterbrock (1987), for several emission-line regions. Since we lack the ratio [O III] λ5007/Hβ for some regions, we also show a combination of diagrams based on emission-line ratios detected in the red only. The thick solid curve tracks a semiempirical dividing line between thermal (H II regions photoionized by hot stars) and nonthermal (shock heated or photoionized by a power-law spectrum) ionization mechanisms (Osterbrock 1989). Generally speaking, all single-component emitting regions show line ratios consistent with photoionization by stars, although several regions are located in a borderline position because of their rather high [S II] $\lambda\lambda$6717, 6730/Hα ratio.

The analysis is more complex for the multicomponent lines where the dominant ionization source may be nonstellar. The ratio [O III] λ5007/H$\beta \lesssim 1$ indicates an ionization level too low for classical AGNs; in fact, A, B, and D have almost LINER spectra with [S II] $\lambda\lambda$6716, 6731/Hα, and [O I] λ6300/Hα too high to be due to H II regions, but with component [4] closer to the ratios typical of H II regions than component [1], at least on A and B (Table 2). Photoionization by a hidden AGN cannot be responsible for the extended nonthermal emission observed at P.A. = 8° without violating the observed line intensities, since maintaining nearly constant Γ would require a corresponding drop in plasma density and, therefore, in emitted surface brightness between the nucleus and off-nuclear regions, which is not seen. A compact source of ionizing photons, like an AGN, would also produce a gradient in excitation degree and line luminosity as a function of radius in the extended emitting region. The ratio [O III] λ5007/H$\beta \sim 1$ occurs both at A and in the surrounding region as far as 10″ radius. We do *not* observe very high ionization gas ([O III] λ5007/H$\beta \gg 1$) anywhere in the galaxy. Both findings suggest that the ionization source is most probably provided in situ. Photoionization by hot stars in a dense medium has been proposed to explain the occurrence of LINERS in early-type galaxies, where the interstellar pressure can be high (Shields 1992). Although this may be the case for A, it is not easy to invoke densities as high as $n_e \sim 10^{5.5}$ cm^{-3} in a more extended region in a spiral galaxy. Shock heating therefore seems the most plausible mechanism for the extended emission at P.A. = 8° (which samples most of the regions of multiple line components).

A comparison between the observed and predicted line ratios computed by models of radiative shocks (Binette, Dopita, & Tuohy 1985) shows that several components have ratios close to the values expected for gas heated by a slow shock $v_s \approx 86$ km s^{-1}, with postshock temperature $T_e \approx 10^{5.2}$ K, and maximum postshock density of 170 cm^{-3} (model B52 of Binette et al. and model D of Shull & McKee 1979). Under these conditions, the predicted line ratios are [O III] λ5007 $\sim$ 1, [N II] λ6583/H$\alpha \sim 0.65$, [S II] $\lambda\lambda$6716, 6713/H$\alpha \sim 1.33$, and [O I] λ6300/H$\alpha \sim 0.44$ which are rather close to the observed values. Shock velocities up to $\sim$200 km s^{-1} give plausible line

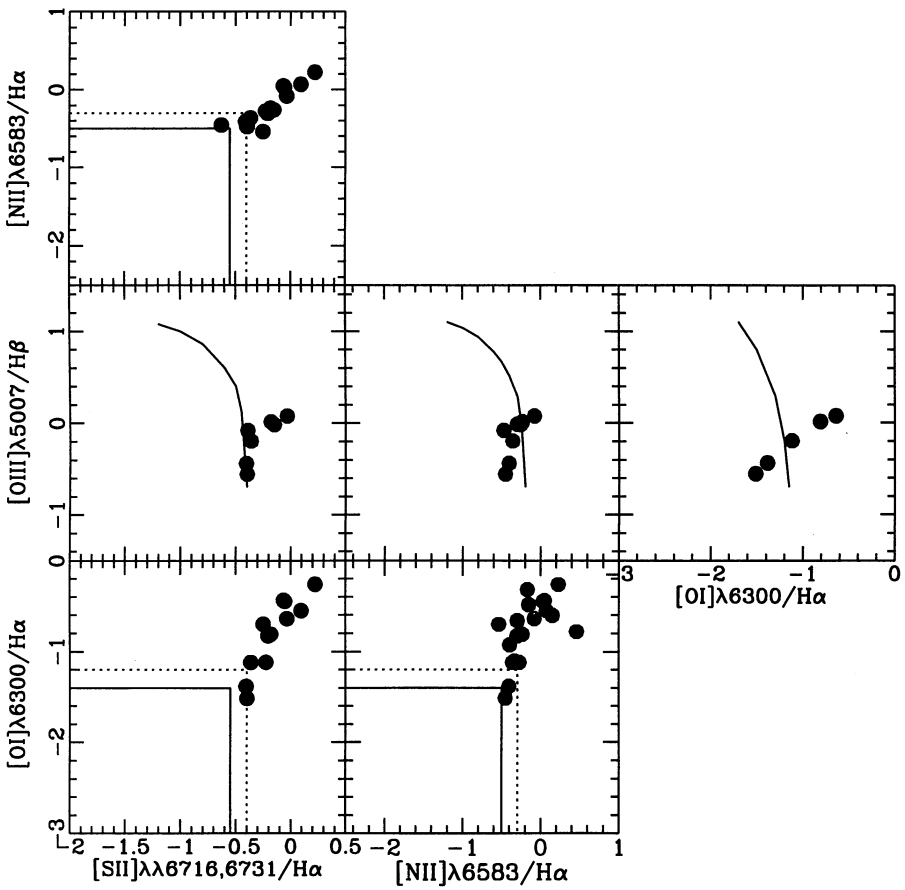

FIG. 9.—Diagnostic diagrams for the emitting regions and line components [1] and [4] of S. Emission-line ratios are plotted in logarithmic scales. Thick solid lines mark the boundary between H II regions (thermal) and nonstellar ionized nebulae (shock heated or NLR-like); the dotted line is a $+2\,\sigma$ boundary.

ratios. Hence moderate velocity shocks could be the sole ionizing source.

4.2. *The Galaxy Masses*

The mass of E is probably equal to or greater than that of S. Assuming a mass-to-light ratio $M/L_B = 8$ for E and 3 for S (e.g., Faber & Gallagher 1979), we estimate from the face-on luminosity $M_{\rm Spiral} \approx 2.1 \times 10^{11}\ h^{-2}\ M_\odot$, and $M_{\rm Ell} \approx 2.5 \times 10^{11}\ h^{-2}\ M_\odot$. Assuming that the v_r curve on the western side of the galaxy is due to rotational motion, we obtain $M_{\rm Spiral} \sim 1.1 \times 10^{11}\ h^{-2}\ M_\odot$ within $d \approx 17.2\ h^{-1}$ kpc. The dynamical mass of the elliptical is $M \approx 2R\langle\sigma^2\rangle/G \approx 2.5 \times 10^{11}\ h^{-2}\ M_\odot$. Given the uncertainties in the mass estimates (about a factor 2), we assume that the masses of E and S are comparable. The line of sight component velocity difference of ~ 700 km s^{-1} suggests that the two galaxies form a bound system only if the total mass if $M \gtrsim 1.2 \times 10^{12}\ M_\odot$, or a factor $\gtrsim 5$ larger than the value estimated above. We note in passing that a bound system including CPG 29 and Mrk 983 would have mass $M_{\rm All\ Bound} \gtrsim 1.60 \times 10^{12}\ h^{-1}\ M_\odot$. This value is not implausible, if compared to the dark matter amount estimated for other groups of galaxies.

4.3. *Clues to the Star Formation History*

The optical continuum of A rises to the blue to our spectral limit of ~ 4400 Å. Such an increase is not usually observed in spiral galaxies of type Sc and luminosity class I (although blue spectra are frequently observed in the luminosity classes from II to V; Bica & Alloin 1987). We ascribe the blue spectral excess (see Fig. 8) to an enhancement in the young stellar population (e.g., a starburst component). We subtracted the continuum spectrum of a typical Sc I galaxy (NGC 692) from the spectrum of A in order to isolate the starburst component (the dotted line in Fig. 8 shows the *adopted* continuum of the old stellar component). Only a few heuristic considerations are possible from our data.

The blue continuum excess and the presence of strong absorption underlying the Hβ emission line suggest that the integrated spectral type of the starburst component is earlier than A5. Assuming that only A0 stars contribute to the starburst spectrum at $\lambda \sim 4800$ Å, $\sim 10^8$ A0 stars are needed to produce the continuum luminosity of the starburst component. Given an initial mass function $\Psi(m) \propto m^{-\alpha}$, with $\alpha \approx 2.5$, the number of O–B stars produced (10–50 $M_\odot$) is n(O–B) ≈ 0.13 n(A). The duration of the starburst must be much longer than the main-sequence lifetime of O–B stars $\tau_{\rm ms,OB} \sim 5 \times 10^6$ yr; otherwise the Hα luminosity $L(\mathrm{H}\alpha)_{\rm SF}$ would be a factor 10^2 larger than observed, assuming a gas covering factor $f_c \approx 0.1$. We can infer that the SFR must have faded in the last 5×10^6 yr, and that the duration of the starburst might be not longer than the main-sequence lifetime of A0 stars $\tau_{\rm A0} \sim 10^8$ yr. The total stellar mass contributed by the starburst in $\sim 10^8$ yr would be $\gtrsim 10^9\ M_\odot$.

Region R is a site of strong off-nuclear star formation. The Hα luminosity in the western line-emitting regions suggests a SFR of $\approx 1.5\ M_\odot$ yr^{-1} adopting the IMF used above (e.g., Bushouse 1987).

5. DISCUSSION

The challenge in understanding CPG 29 centers on explaining the velocity excesses up to 1300 km s^{-1} that the emission-line components north of the nucleus show relative to the redshift of the S nucleus. We explore four possible interpretations for the peculiarities observed in S including both interaction and internal mechanisms.

5.1. *Interpretation 1: The Spiral as an FIR-strong Galaxy*

Large internal velocity ranges with split emission-line profiles have been observed in the most powerful *IRAS* (hereafter FIR-strong) galaxies. The degree of complexity observed in the blend Hα + [N II] $\lambda\lambda$6548, 6583 is comparable to that observed in NGC 3079 (Heckman et al. 1990) and in IRAS 19254+7245 (Colina, Lipari, & Macchetto 1991). The diagnostic emission-line ratios are similar to the ones observed in strong FIR emitters (e.g., Heckman et al. 1990).

The FIR luminosity of S derived from *IRAS* ADDSCAN data is $L_{\rm FIR} \approx 2.6 \times 10^{10}\ h^{-2}\ L_{\odot}$ (we neglect any contribution from the elliptical component which is likely to be negligible). This is about 8 times the average for the ES pairs listed in the CPG (Xu & Sulentic 1991). This value is also larger than those observed for the prototypical starburst galaxies NGC 253 and M82. The inclination-corrected magnitude for S is $m_{0T} \approx 14.20$ (RC3) which corresponds to $L_B \approx 5 \times 10^9\ h^{-2}\ L_{\odot}$. The ratio $L_{\rm FIR}/L_B$ is therefore $\approx$4.6, again larger than the value for NGC 253, but lower than the values observed in the most powerful FIR galaxies. The color ratio $f_{60\,\mu m}/f_{100\,\mu m} \sim 0.30$ implies a dust temperature of $\approx$47 °K, lower than that observed in most FIR galaxies. The values of $L_{\rm FIR}$, of $f_{60\,\mu m}/f_{100\,\mu m}$, and of $L_{\rm FIR}/L_B$ place S at the low-power end of the strong FIR emitters studied by Heckman et al. (1990). The low $f_{60\,\mu m}/f_{100\,\mu m}$ ratio is not atypical of late-type normal spirals.

Large-scale bipolar outflows along the disk rotation axis, as found in such FIR-strong galaxies as NGC 253, 3628, and 6240, would give rise to both blue- and redshifted emission-line components. The opacity of the disk could suppress the blueshifted emission if the outflow were close to the disk plane and the disk were properly warped. The extinction in the disk of the galaxy should be $A_V \gtrsim 4.5$ mag to dim the blueshifted Hα emission down to the 3 σ level (under the assumption that the redshifted emission line components are not obscured). White & Keel (1993) and James & Puxley (1993) recently estimated that the disk opacity of face-on Sb–Sc galaxies should only give $A_V \lesssim 1.8$ mag. The appearance and inferred inclination of S makes a value as large as 4.5 a not unlikely possibility. However, the total Δv_r (i.e., including the obscured blueshifted component) should be $\approx$2600 km s^{-1}, which exceeds the value observed in all of the most powerful FIR galaxies. The dimming of the blueshifted component of an outflow would require a conspiracy of two extreme conditions—outflow close to the disk plane and warping of the disk so that only the redshifted outflow remains unobscured.

5.2. *Interpretation 2: Interaction with the Intergalactic Medium*

This is a relatively old idea (e.g., Freeman & de Vaucouleurs 1974) more recently discussed by Combes et al. (1988) in a context similar to CPG 29. It was recently revived by the discovery of diffuse X-ray emission in the NGC 2276/2300 "group" of galaxies (Mulchaey et al. 1993) which is dominated by the relatively isolated E + S pair CPG 127 (Arp 114). One could hypothesize that S is passing through a region where the ram pressure of a relatively dense intergalactic medium is stimulating star formation and shocks. The compressed appearance of the bright arm on the northern edge of S is suggestive of such an effect. Mulchaey et al. (1993) also suggest that the peculiar optical morphology of NGC 2276 is due to an ongoing intragroup medium–galaxy encounter. This interpretation must remain speculative until H I or X-ray data become available for the neighborhood of CPG 29.

5.3. *Interpretation 3: Interaction Involving a Third Party*

While we cannot rule out the possibility of a third galaxy, it appears to be well concealed. An observation possibly favoring the existence of a third small galaxy close to S is that emission-line ratios in C and component [4] of B are consistent with H II regions. B might be identified with the small companion. However, component C appears too diffuse while B shows at best a weak continuum. The H I data for CPG 29 (Bothun et al. 1983) also shows an emission profile consistent with a single gas-rich galaxy.

5.4. *Interpretation 4: Pole-on Collision between Spiral and Elliptical*

5.4.1. *Morphology: An Emerging Ring Galaxy?*

Two ringlike features are easily visible on the CCD image of S (Fig. 1 and § 3.1). These features can be produced by a polar or nearly polar encounter, in principle either with the elliptical, or with a hypothetical third party (e.g., Toomre & Toomre 1972; Theys & Spiegel 1977; Appleton & Struck-Marcell 1987). Numerical simulations and physical intuition suggest that a primary ring should start forming at the time the intruder crosses the target galaxy; assuming that the plane of the orbit is inclined $i \approx 45°$ to the line of sight, the separation time between spiral and elliptical and the order-of-magnitude expansion times (in years) for the (three?) rings are as follows:

$$\tau_{\rm Ell,Spiral} = 5.2 \times 10^7\ \Delta v^{-1}_{\rm Ell\text{-}Spiral,1000}\ ,$$

$$\tau_{\rm in} = 4.0 \times 10^7\ v^{-1}_{\rm in,100}\ ,$$

$$\tau_{\rm inter} = 9.4 \times 10^7\ v^{-1}_{\rm inter,100}\ ,$$

$$\tau_{\rm outer} = 2.4 \times 10^8\ v^{-1}_{\rm out,100}\ .$$

The expansion velocity of the primary ring should be $\approx \frac{1}{2}\,\Delta v_{\rm Ell\text{-}Spiral}$; the outermost "ring," i.e., the line of knots at the southern edge of the galaxy, and a faint northeastern arc should be associated with the "aged" primary ring since $\tau_{\rm out} \approx 4.8 \times 10^7$ yr $\approx \tau_{\rm Ell,Spiral}$.

Hydrodynamical models (Appleton & Struck-Marcell 1987; Appleton & James 1990) suggest that the leading edge of the primary ring should be a site of strong star formation. The secondary ring should show even stronger star formation due to a large degree of compression in the density wave; star formation should then fade with increasing ring order. This scenario agrees with the star formation properties of the ring-like features observed in S (in the simplest picture of a single passage): (1) no evidence of Hα emission in the innermost ring and (2) strongest star formation in the bright arc of the intermediate ring. Little can be said about the outermost line of knots that skirts the southern edge of S but it seems reasonable to suppose that they are H II regions.

The northern side of the intermediate ring (the bright arc, or R) is much brighter than the southern one; this probably implies that the encounter between the spiral and the elliptical was mildly off-center (impact parameter $\lesssim$6″). Gerber, Lamb, & Balsara (1992) attempted to reproduce the morphology of

Arp 147 through numerical simulations of the slightly off-center polar encounter of two galaxies of equal mass. Their simulations produced a feature that, once projection effects are accounted for, can be equated to the *bright arc* of S. In the innermost regions of S ($\lesssim 6''$), the motion of the nucleus across the galactic disk may have contributed to the creation of a surrounding shock-heated region and, even, to the double-peaked appearance of the nuclear region in the Hα image. We note that the morphology of the line-emitting gas is markedly different from that of the stellar component. Simulating separately gaseous and stellar components in head-on encounters, Horellou & Combes (1993) showed that gas can be removed from one of the colliders: gas would accelerate at high velocities toward the intruder (after its passage), creating a vertically displaced structure, while the stellar component does not, in agreement with what we observe in CPG 29.

5.4.2. *Simulations: Could the Elliptical Emerge Unscathed?*

Evidence for strong interaction in ellipticals often includes a displacement of the outer isophotal centroid towards the companion; the side closest to the companion is often distended, while the opposite side is compressed (Borne 1988). From the analysis of § 3.1, we can conclude that E shows little, if any, evidence for significant tidal perturbation. Small deviations from an $r^{1/4}$ law are frequently observed in ellipticals, although their significance with reference to the interaction history is not clear (Kormendy & Djorgovski 1989).

We carried out numerical simulations of the pair, employing the *N*-body (NBODY2) code written by S. Aarseth. Our aim was not to reproduce satisfactorily the observed morphology of S but rather to study whether the elliptical can emerge unscathed by the pole-on or nearly pole-on crossing of the spiral.

We used ≈1200 particles for each galaxy in each simulation; we modeled S as a flat exponential disk with *e*-folding scale 1.5–2.5 kpc; the elliptical was represented as a modified isothermal spheroid (King radius 3 kpc) supported by anisotropic velocity dispersion. The stability of both spiral and elliptical was studied in several control runs in which both galaxies were allowed to evolve as isolated objects. We assumed that the two galaxies have the same mass, $M \approx 2.5 \times 10^{11}\ M_\odot$. We simulated various encounters for different choices of the inclination ($i = 0°, 15°$) and of the initial approaching velocity, and for two values of the impact parameter (0″ and 6″). For $\Delta v_{\rm Ell\text{-}Sp} \approx 1000$ and 700 km s^{-1} the elliptical is not affected by the crossing of the spiral. This result of our simulations has been confirmed by more sophisticated simulations of head-on elliptical/spiral encounters performed employing the TREECODE by L. Hernquist. The simulations (A. Curir 1993, private communication) show that a 5000 particle King sphere hitting a 3000 star target disk is not affected when $\Delta v_{\rm Ell\text{-}Spi} \approx 1000$ km s^{-1}. The TREECODE simulations also reproduce very well the bright arc seen in S (Curir & Filippi 1994).

We will suggest in the next section how a collision between E and S can easily explain both moderate velocity shocks and large internal Δv_r in S.

5.4.3. *The Shock-heated Gas*

The H II–like line ratios in C can be explained if the gas has been stripped and accelerated toward E. The acceleration of molecular gas clouds depends upon time, because of the varying potential of the approaching, crossing, and then receding elliptical galaxy. The clouds accelerated to the highest velocity will not collide with other clouds. If clouds accelerate to a velocity $v_1 > v_2$ at $t_1 > t_2$, then the velocity difference could make a cloud-cloud collision possible at a moderate velocity $v_{12} \approx v_1 - v_2 \sim 100$ km s^{-1}.

Cloud-cloud collisions are therefore a likely agent in the production of shock-heated gas for line components [1]–[3] in **B** and possibly A. If the thickness of the clouds is $\Delta s \approx 2.7 \times 10^{20}$ cm, the clouds are destroyed in a time $t \approx 8.6 \times 10^5 v_{12,100}^{-1}$ yr. Shock production is thus sustained for an appreciable amount of time. The $\Delta v_r \sim 1300$ km s^{-1} in S, is much larger than the radial velocity difference between the components (750 km s^{-1}). This does not demand that a third galaxy is responsible for the disk collision; rather, it demands that part of the orbital energy be transferred to the stripped molecular clouds.

Models with shock velocity higher than 250 km s^{-1} do not agree with the line ratios observed in S. However, shock-heating emission may be diluted by photoionization by OB stars; in which case more extreme shock velocities could be appropriate. Caution is needed in converting between observed line velocities and expected shock velocities, since the latter are strictly local and may, for example, reflect shocks driven into individual clouds rather than large-scale phenomena characterized by the large-velocity splitting between emission-line components.

The models of Binette et al. (1985) give an Hα luminosity per unit shock transversal area $L(\mathrm{H}\alpha)/\Sigma = 3.9 \times 10^{-5} v_{100}^{1.48}$ ergs s^{-1} cm^{-2}. A typical giant molecular cloud in the solar neighborhood has mean diameter ≈45 pc, or a projected surface area $\Sigma \approx 2.1 \times 10^3$ pc^2; if two molecular clouds of this size collide with $\Delta v \approx 100$ km s^{-1}, we will have $L(\mathrm{H}\alpha) \approx 2 \times 10^{40}$ ergs s^{-1} $\times\ L(\mathrm{H}\alpha)/\Sigma \times (t_{\rm cool}/t_{\rm dyn}) \approx 1.710^{37} \times v_{100}^{4.94}$ ergs s^{-1} $\approx 4.4 \times 10^3 v_{100}^{4.94}\ L_\odot$, where the ratio $t_{\rm cool}$ is the cooling time, and $t_{\rm dyn}$ is the time needed by the shock front to cover a distance equal to the thickness of one cooling layer in the post-shock zone. The $L(\mathrm{H}\alpha)$ of the emitting regions where shock heating is the dominant ionization mechanism is $\sim 1 \times 10^{41}\ h^{-2}$ ergs s^{-1} $\approx 2.6 \times 10^7\ h^{-2}\ L_\odot$. The equivalent of ~10 giant molecular clouds must be presently colliding in S in order to produce the observed $L(\mathrm{H}\alpha)$ if $v \sim 200$ km s^{-1}. Assuming that each cloud has a thickness of 60 pc, and that the average density in the clouds is ~100 cm^{-3}, the mass of molecular gas needed to sustain the Hα emission is $M_{\rm H_2} \approx 1.2 \times 10^7\ h^{-2}\ M_\odot$.

At face value, the observed $L_{\rm FIR}$ implies a current SFR of 13 $M_\odot$ yr^{-1}; however, shock-heated gas may be responsible for an enhancement of FIR luminosity as well (e.g., Harwit et al. 1987). Equating the kinetic energy dissipated in the intracloud collision to the $L_{\rm FIR}$ observed for S requires a mass $M \approx 2.12 \times 10^{10} Z_{60} L_{10} v_{100}^{-3}\ M_\odot$. The molecular content of an entire galactic disk must be involved in the collision unless the velocity of approach is much larger than 100 km s^{-1}: only a violent collision with a hypothesized third party, with $\Delta v \approx 1000$ km s^{-1}, would change the estimate in favor of shock heating explanation for $L_{\rm FIR}$. If we ascribe the Hα emission to shock-heated gas in a layer between colliding molecular clouds stripped by E, then only a negligible fraction $\ll 1$ of $L_{\rm FIR}$ can be due to shock-heated gas, and $L_{\rm FIR}$ can be safely ascribed to star formation alone.

5.4.4. *The Problems with the Pole-on Collisions*

There are some difficulties for this simple scenario. A preliminary analysis of the velocity curves at P.A. = 81° suggest that the velocity field deduced from line component [1] could be entirely rotational on the west side of S (§ 3.3). Results are qualitatively in agreement with the double-wave model *only* if

the systemic radial velocity is $v_{r,sys} \approx 14{,}260$ km s^{-1}; otherwise a double-wave fit is not possible. We do not observe evidence of expansion velocities as large as 500 km s^{-1}. As shown previously, radial velocity differences on the western side of S do not exceed 150 km s^{-1}.

6. CONCLUSIONS AND IMPLICATIONS

We have presented images and spectra of the mixed morphology galaxy pair CPG 29. The most unusual feature is the complex extended line emission activity in S. Our resolution of the emission lines into multiple components has provided clues to the nature of this system. We have shown that the morphology of S can be explained if S is a ring galaxy emerging from a near pole-on encounter with E. Knots B and C probably represent tidally stripped gas rather than a second nucleus or a smaller, third galaxy. The large internal velocity difference of 1300 km s^{-1}, and the shocked gas conditions in S probably result from the acceleration of the line-emitting gas by gravitational forces.

The results for S raise the possibility that the acceleration of gas in superwind galaxies might be gravitational in origin, instead of being produced by the collective effort of "organized" supernovae. A favorable orientation for the orbit of the companion, along with multiple passages, might produce a two-way streaming of gas. This point is speculative, but it should be investigated before any conclusion on the origin of optical line emission in strong FIR galaxies is reached. This is especially true since the most powerful FIR galaxies are probably merging spirals. For instance, S is kin to NGC 1143, a FIR-strong spiral galaxy with a Seyfert 2 nucleus that has probably been crossed by a less massive elliptical companion. We can identify several similarities between the morphology of the two galaxies. A picture of NGC 1144 has been published by Hippelein (1989, Fig. 1). This author noted that *the internal velocity differences in NGC* 1143 *are extremely high*, with $\Delta v_r \gtrsim 1000$ km s^{-1}. The largest value of the velocity gradient is, interestingly enough, observed close to the major axis of the pair. We suggest, in analogy with S, that the large Δv_r may not be indicative of rotational motion, and hence of large mass concentration, but rather be related to the stripping exerted by the elliptical during a collision with the spiral.

Hernquist (1989) showed that strong interaction is able to channel $\sim 10^9\ M_\odot$ of gas within the innermost $d \sim 200$ pc. The fate of the gas at $d \lesssim 200$ pc is still unclear. Probably barlike instabilities are then able to funnel the gas toward the innermost pc (Shlosman, Frank, & Begelman 1989). It is important to stress that we oberve strong emission-line activity but little or no evidence for nonthermal nuclear activity. Heuristic consideration suggest that an *aged* nuclear starburst may have produced a total mass of $\sim 10^9\ M_\odot$. This finding may suggest that the barlike instability supposed to channel the gas to $d \lesssim 1$ pc is governed by the global galactic potential and does not operate in galaxies of late morphological type (e.g., Noguchi 1991).

D. D.-H. and P. M. acknowledge the financial support of the University of Alabama, and the support of the SPM Observatory staff, that allowed one successful observing run. We acknowledge support from EPSCoR grant EHR-9108761. D. D.-H. acknowledges support from grant IN451091 from DGAPA, UNAM. Observations at the 6 m telescope were supported by the NSF under the Large Foreign Telescopes program. We thank Anna Curir for the simulation performed.

REFERENCES

Afanasiev, A. L., Vlasiuk, V., Dodonov, S., & Sil'chenko, O. K. 1990; Spets. Astrofiz. Obs. preprint
Appleton, P. N., & James, R. A. 1990, in Dynamics & Interaction of Galaxies ed. R. Wielen (Berlin: Springer-Verlag), 200
Appleton, P. N., & Struck-Marcell, C. 1987, ApJ, 318, 103
Arp, H. 1966, ApJS, 14, 247
Artyukh, V. S., Kandalyan, R. A., Hovanissian, M. A., & Sanamyan, V. A. 1982, Astrofizika, 18, 215
Bica, E., & Alloin, D. 1987, A&AS, 70, 281
Binette, L., Dopita, M. A., & Tuohy, I. R. 1985, ApJ, 297, 476
Borne, K. 1988, ApJ, 330, 61
Bothun, G. D., Heckman, T. M., Schommer, R. A., & Balick, B. 1984, AJ, 89, 12
Bushouse, H. 1987, ApJ, 320, 49
Colina, L., Lipari, S., & Macchetto, F. 1991, ApJ, 379, 113
Combes, F., Dupraz, C., Casoli, F., & Pagani, L. 1988, A&A, 203, L9
Curir, A., & Filippi, R. 1994, A&A, submitted
Dahari, O. 1985, ApJS, 57, 643
Dahari, O., & De Robertis, M. M. 1988, ApJS, 67, 249
de Vaucouleur, G., de Vaucouler, A., Corwin, H. G., Jr., Buta, R. J., Paturel, G., & Fouque, P. 1991, Third Reference Catalogue of Bright Galaxies (New York: Springer-Verlag) (RC3)
Elmegreen, D. M., Elmegreen, B. G., & Bellin, A. D. 1991, ApJ, 364, 415
Faber, S. M., & Gallagher, J. F. 1979, ARA&A, 17, 135
Freeman, K. C., & de Vaucouleurs, G. 1974, ApJ, 194, 569
Gerber, R. A., Lamb, S. A., & Balsara, D. S. 1992, ApJ, 399, L51
Harwit, M., Houck, J. R., Soifer, B. T., & Palumbo, G. G. C. 1987, ApJ, 315, 28
Heckman, T. M., Lehnert, M. D., & Armus, L. 1993, STScI preprint 724
Hernquist, L. 1989, Nature, 340, 687
Hippelein, H. H. 1989, A&A, 216, 11
Horellou, C., & Combes, F. 1993, in *N*-Body Problems and Gravitational Dynamics, ed. F. Combes & E. Athanassoula (Paris: Observatoire de Paris), 168
James, P. A., & Puxley, P. J. 1993, Nature, 363, 240
Karachentsev, I. D. 1972, Catalogue of Isolated Pairs of Galaxies in the Northern Hemisphere, Soobshch. Spets. Astrfiz. Obs. 7, 3
———. 1980, ApJS, 44, 137
———. 1987, Double Galaxies (Moscow: Nauka)
Karachentsev, I. D., Sargent, W. L. W., & Zimmermann, B. 1979, Astrophysics, 15, 19
Kennicutt, R. C., Roettiger, K. A., Keel, W. C., van der Hulst, J. M., & Hummel, E. 1987, in Star Formation in Galaxies (NASA Conf. Pub. 2466), ed. C. J. Lonsdale Persson, 401
Kormendy, J., & Djorgovski, G. 1989, ARA&A, 27, 235
Larson, R., & Tinsley, B. M. 1978, ApJ, 219, 46
Lynds, R., & Toomre, A. 1976, ApJ, 209, 382
Mazzarella, J. M., & Boroson, T. A. 1993, ApJS, 85, 27
Mazzarella, J. M., Bothun, G. D., & Boroson, T. A. 1991, AJ, 101, 2034
Mulchaey, J. S., Davis, D. S., Mushotzky, R. F., & Burstein, D. 1993, ApJ, 404, L9
Noguchi, M. 1994, in Mass Transfer Induced Activity in Galaxies, ed. I. Shlosman (Cambridge: Cambridge Univ. Press), 251
Norman, C., & Scoville, N. Z. 1988, ApJ, 332, 124
Osterbrock, D. E. 1978, Phys. Scripta, 17, 137
———. 1989, Astrophysics of Gaseous Nebulae and Active Galactic Nuclei (Mill Valley: University Science Books)
Osterbrock, D. E., & Dahari, O. 1983, ApJ, 273, 478 (OD83)
Palumbo, G. C. G., Tanzella-Nitti, G., & Vettolani, G. 1983, Catalog of Radial Velocities of Galaxies (New York: Gordon & Breach)
Rafanelli, P., & Marziani, P. 1992, in Morphological and Physical Classification of Galaxies, ed. G. Busarcello, et al. (New York: Springer-Verlag), 451
Shields, J. C. 1992, ApJ, 399, L27
Shlosman, I., Frank, J., & Begelman, M. C. 1989, Nature, 338, 45
Shull, J. M., & McKee, C. F. 1979, ApJ, 227, 122
Sulentic, J. W. 1976, ApJ, 213, 327
Theys, J. C., & Spiegel, E. A. 1977, ApJ, 212, 616
Tifft, W. G. 1982, ApJS, 50, 319
Toomre, A., & Toomre, J. 1972, ApJ, 178, 623
Veilleux, S., & Osterbrock, D. E. 1987, ApJS, 63, 295
Weedman, D. W. 1983, ApJ, 266, 479
White, R. E., III, & Keel, W. C. 1993, Nature, 359, 129
Xu, C., & Sulentic, J. W. 1991, ApJ, 374, 407